Design of a Traveling Wave Thermoacoustic Engine Driven Cooler with Hybrid Configuration

Ali Al-Kayiem and Zhibin Yu*

***Abstract*— Kees de Blok proposed a "hybrid configuration" travelling wave thermoacoustic engine and his prototype using atmosphere air as the working gas achieved an onset temperature difference as low as 65 K. However, no further research work has been reported on this type of thermoacoustic engine to reveal whether this type of engine can achieve higher efficiency, or how to couple it with acoustic loads such as a thermoacoustic cooler or a linear alternator. This paper investigates these problems based on a series of comprehensive numerical simulations. A numerical model is established using the reported parameters and validated by the published data. The physical principles behind the design were then understood in detail. The validated model is then modified and an acoustic load (i.e., a thermoacoustic cooler) is installed to the engine. The simulation results show that the engine can achieve about 46.5% of the Carnot efficiency and the cooler can achieve 39.6% of Carnot COP. The research of this paper shows that this new engine configuration has the potential to achieve high efficiency.**

***Key words*— thermoacoustic engine, travelling wave, cooler, resonator**

I. INTRODUCTION

Thermoacoustic engines deals with the thermodynamic conversion between thermal energy and acoustic work (i.e. a p-v work). In 1979, Ceperley [1, 2] pointed out that, when the travelling sound wave propagates through a regenerator with positive temperature gradient along the direction of sound wave propagation, the gas parcel within the regenerator experiences a Stirling-like thermodynamic cycle, and therefore a travelling wave thermoacoustic engine can be built. Yazaki et al. [4] demonstrated a practical travelling-wave thermoacoustic engine for the first time, which however had a relative low efficiency because of the large viscous losses resulting from high acoustic velocities in the regenerator and the resonator feedback. Backhaus and Swift [5] later invented a travelling wave thermoacoustic Stirling engine. The thermoacoustic core was placed within a torus with a length much shorter than the acoustic wavelength at the operating frequency. A long standing-wave resonator was connected to this torus just after the secondary ambient heat exchanger to provide the resonance.

Author Ali Al-Kayiem Support from the Ministry of Higher of Education/ Babylon University in Iraq (No. 553 Iraqi cultural attaché). Ali Al-Kayiem is with the School of Engineering, University of Glasgow, Glasgow, Scotland, United Kingdom; e-mail: a.al-kayiem.1@research.gla.ac.uk
*Corresponding author: Zhibin Yu is with the School of Engineering, University of Glasgow, Glasgow, Scotland, United Kingdom;e-mail:Zhibin.Yu@glasgow.ac.uk

Backhaus' engine achieved a thermal efficiency of 30%, equivalent to 41% of the theoretical Carnot efficiency. Tijani and Spoelstra [6] later designed and built a similar thermoacoustic Stirling heat engine, and achieved 49% of Carnot efficiency.

Kees de Blok has made a series of efforts on the development of travelling wave thermoacoustic engines [7, 8, 10]. He proposed a bypass type traveling-wave thermoacoustic engine in 1998, which operates on similar principles to the thermoacoustic Stirling engine developed by Backhaus [5]. In 2008, he proposed a hybrid configuration for travelling wave thermoacoustic engine, which lowered the onset temperature difference to about 65 K and demonstrated a great potential for utilising low temperature heat sources such as solar energy and waste heat sources [7]. Later, he also demonstrated multistage looped type travelling wave thermoacoustic engines, and their applications to drive coolers and linear alternators [3]. It was pointed out that, in theory an arbitrary number of thermoacoustic engine units can be connected in series within one looped tube resonator. However, the 4-stage configuration has a unique advantage because the four engine units can be placed with equal distance within the loop so that the distance between two adjacent stages is about one quarter of the wave length. In this way, the reflections due to impedance anomalies tend to compensate each other. Therefore, near travelling wave conditions can be achieved within the regenerators and feedback pipe.

Essentially, the various engine types mentioned above all work on the same thermodynamic principle. The different configurations mainly lie in the different designs of acoustic resonator. The resonator provides the acoustic resonance to facilitate the gas parcel to complete the thermodynamic cycle with the regenerator. Depending on the characteristics of the acoustic field within the resonator, it can be a standing wave or travelling wave resonator. Backhaus' thermoacoustic Stirling engine used a quarter-wave-length standing wave resonator. Yazaki's engine and de Blok's' multistage engine used a one-wave-length travelling wave resonator. De Blok's' hybrid configuration engine used a travelling wave resonator with a bypass.

The design principle of a thermoacoustic engine is to maximize the acoustic power generation within the thermoacoustic core, while minimising the acoustic loss within the acoustic resonator. The travelling wave resonator is superior to standing wave one as its acoustic loss is much lower. In a standing wave resonator, there is a positive interference between two traveling waves, so that the pressure and velocity local amplitudes can be nearly twice

ISBN: 978-988-19253-5-0
ISSN: 2078-0958 (Print); ISSN: 2078-0966 (Online)

the amplitudes in the initial traveling wave generated in the engine, resulting in high acoustic losses [3].

As schematically shown in Fig.1, the hybrid configuration thermoacoustic engine proposed by de Blok has achieved a very low onset temperature difference. However, there is no further research on this type of engine to clarify whether this type of engine can potentially achieve high thermodynamic efficiency compared with other type of travelling wave thermoacoustic engines. It also remains unknown how the acoustic load can be installed to such engine without altering the delicately designed acoustic field.

This paper aims to answer some of these questions based on a series of comprehensive simulations. Firstly, a numerical model is established based on the information reported in the references, and then the model is validated against reported experimental data. Once the model is validated, the design principle is fully understood. The model is then modified and acoustic load is installed to the engine carefully without breaking the design principles. In this way, a hybrid configuration thermoacoustic engine driven cooler will be modelled to investigate how high an engine efficiency can be obtained, and how the acoustic load (i.e. cooler) can be coupled to the engine. The results are presented and discussed in detail in this paper.

II. MODEL AND VALIDATION

The hybrid configuration thermoacoustic engine proto type reported by de Blok is modelled using DeltaEC software (Design Environment for Low-amplitude ThermoAcoustic Energy Conversion). [9] As shown in Figure 1, this engine has two stages, and each stage has a hot heat exchange (HHX), regenerator (REG), and ambient heat exchanger (AHX).

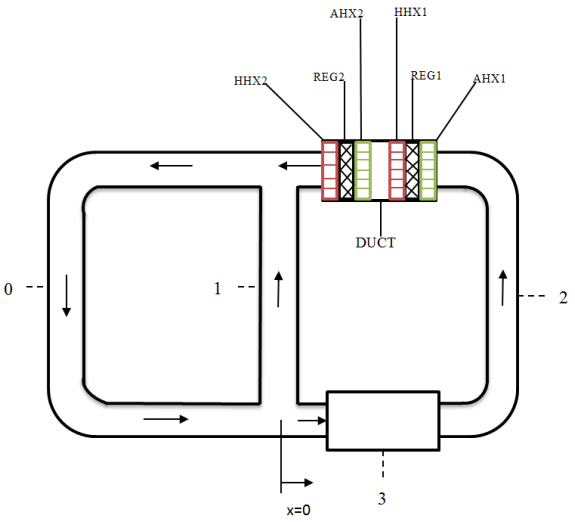

Fig. 1. Schematic diagram of the bypass geometry.

The other components of the system are described as: feedback pipe (0), bypass pipe (1), compliance (3), inertance tube (2), two regenerators, two ambient heat exchanges and two hot heat exchanges. Most of the dimensions were obtained from the reference and listed in Table I, and some dimensions were estimated according to our understanding when they are not directly available from the reference [8]. The working gas is air at atmosphere pressure, and the operating frequency is 117 Hz. The simulations results are shown as Figures 2 -5.

Table I. Dimensions of de Blok' prototype [8].

Part	Diameter (m)	Length (mm)	R_h (um)	Porosity
AHX1	0.123	0.56	40*	0.8
REG1	0.123	1.58	150*	0.74
HHX1	0.123	0.56	120*	0.8
AHX2	0.123	0.56	120*	0.8
REG2	0.123	1.58	130*	0.74
HHX2	0.123	0.56	120*	0.8

Part	Diameter (m)	Length (m)
Bypass	0.075	1*
Resonator	0.075	1.75*
Inertance	0.05	1.2*
Compliance	0.11	0.127*
Duct between two stages	0.123	0.03

*These parameters were not reported in the reference, and are estimated.

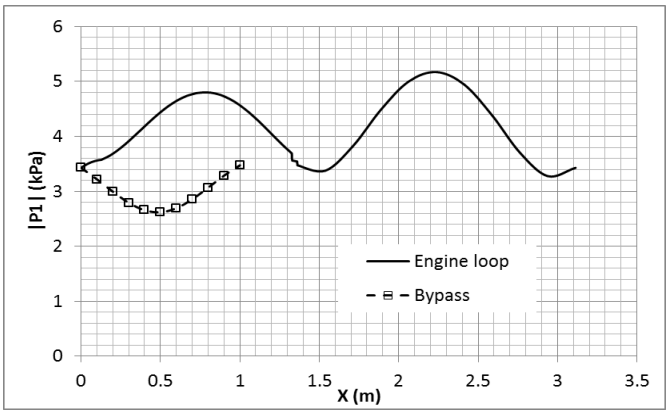

Fig. 2. Distribution of the amplitude of acoustic pressure along the loop.

Table II. Comparison of pressure amplitude at different location.

Location	Measurement (kpa)	Present simulation (kpa)
REG section	5.22	5.2
Resonator	3.54	3.6
Bypass	2.77	2.7
Compliance	4.36	4.7
Inertance	1.87	3.4

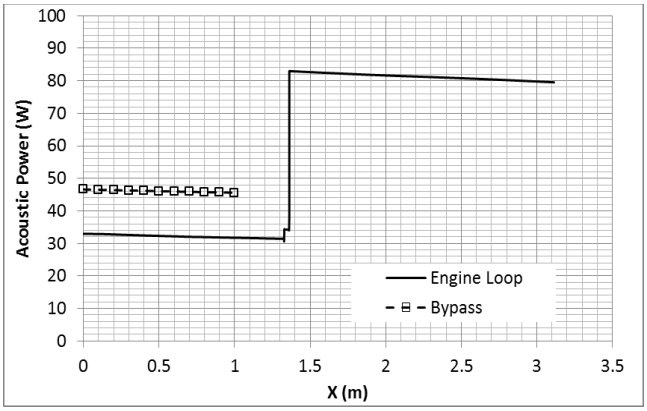

Fig. 3. Distribution of the acoustic power along the loop.

Figure 2 shows the pressure amplitude along the engine loop. The pressure amplitude in the resonator is 3430 Pa and the Standing Wave Ratio (SWR) is about 1.2. In the present simulation, the pressure amplitude is set the same as 3430 Pa in the resonator and the obtained SWR is 1.5. Table II shows the comparison between the simulated results and the reported experimental data. The experimental results agree

ISBN: 978-988-19253-5-0
ISSN: 2078-0958 (Print); ISSN: 2078-0966 (Online)

with the simulation very well, except the pressure amplitude in the inertance tube.

Figure 3 shows the acoustic power distribution along the loop system. The simulation starts from the junction of the bypass and engine branch (X=0). The total acoustic power is about 80 W, and it splits into two parts. One part flows into the bypass and is about 47 W, and the other part is about 33 W and flows into the compliance. The two engine stages slightly amplify the acoustic power to 37 W, which then joins with the acoustic power flow from the bypass pipe. The total power is now about 82 W and flows into the feedback pipe. The feedback pipe transports the acoustic power back to beginning (X=0).

Acoustic power has been measured at two locations as shown in Fig. 1 [8]. The first location P1 lies in the centre of inertance tube and the second location P2 is at the beginning of the feedback pipe. The measurements showed that the acoustic power flow is about 35 W at location P1 and about 78 W at location P2. In the present model, the simulations show an acoustic power of 32 W at location P1 and about 79 W at location P2. The simulation results agree with the measurements very well.

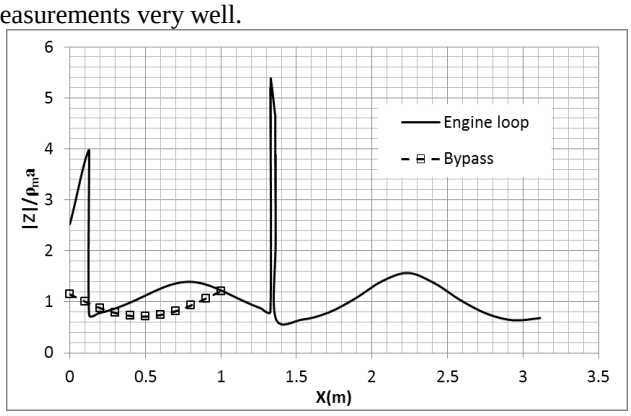

Fig. 4. Distribution of the normalized acoustic impedance along the loop.

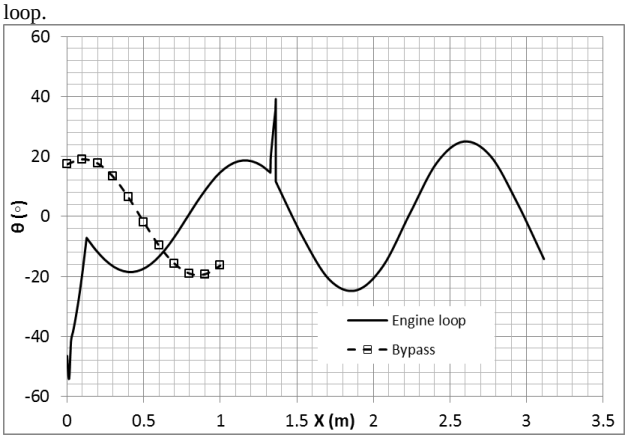

Fig. 5. Phase angle θ between pressure and velocity oscillations along loop.

The design philosophy for this type of engine is that, the acoustic impedance at the end of the feedback pipe (X=0) should be tuned to the characteristic impedance $\rho_m a$ of a pure travelling wave field, so that the reflection can be cancelled. This is very similar to the impedance match technique of a microwave network. In this way, the acoustic power can be transmitted through the feedback pipe with the least losses. To check this design principle, the normalised impedance has been extracted from the simulation results and shown as Fig. 4. It can be found that the acoustic impedance at the end of feedback pipe (X=3.1 m) is about $0.7\rho_m a$, which is very close to 1 as expected. However, due to the lack of some dimensions, the actual impedance measured by de Blok is closer to 1. Notwithstanding, the present model has captured the physics of the prototype.

The normalised impedance increases along the compliance duct from 2.45 to 4, and then sharply drops to 0.7 at the beginning of the inertance tube due to the sudden change of cross sectional area. The normalised impedance in the regenerator is estimated to be around 3 in de Blok's prototype but no measurement is provided, while it is about 5 according to the simulation of the present model. $|Z|/\rho_m a$ is in the range 0.6~1.4 within the feedback pipe, which is not very far from the ideal value of 1 as expected. It is also interesting that $|Z|/\rho_m a$ is about 1 throughout the bypass, which indicates that a near travelling wave condition has been achieved in the bypass as expected.

To further understand the design principle of this type of travelling wave thermoacoustic engine the phase difference between the pressure and velocity oscillation has been extracted and showed in Fig.5. From Fig. 5, it can be found that the by-pass and the feed-back pipe has a phase angle in the range $-20° < \Theta < 20°$, and therefore a near travelling wave field has been achieved in these two main components. From the acoustic viewpoint, these two components actually form the acoustic resonator for the engine. The onset temperature difference is significantly reduced because the travelling wave acoustic resonator dissipates much less acoustic power compared with the standing wave resonator that was used in Backhaus' thermoacoustic engine. The two thermoacoustic engine stages also work at a near travelling wave condition.

However, there is a spike shown in Figure 5 (x=1.28~1.3 m), where is at the end of the inertance tube. This is due to the sudden change in area from a small inertance area to a big engine section. The compliance of the engine section shifted the phase significantly.

III. Application to a Thermally Driven Cooler

The validation of the model offered us the confidence to apply this new configuration travelling wave thermoacoustic engine to some actual applications. In this paper, we aim to develop a thermally driven thermoacoustic refrigerator with an operating temperature about -20 °C. The heat source is in a temperature range 200-300 °C.

The whole system has a similar configure to that shown in Figure 1. However, the second stage engine unit is replaced by a cooler stage, and the regenerator of the engine stage has been increased from 1.58 to 20 mm to utilise a relatively high temperature difference. The working gas is changed to pressurised nitrogen with a pressure of 10 bar. The operating frequency is about 75 Hz. The maximum pressure amplitude is about 85 kPa, and therefore the relative pressure amplitude relative to the men pressure is about 8.5% which is in the range in which the DeltaEC computing programme can be used.

ISBN: 978-988-19253-5-0
ISSN: 2078-0958 (Print); ISSN: 2078-0966 (Online)

The dimensions of the main components are summarized and listed in Table III. The regenerators have the geometric configuration of a mesh screen. Following the same design as de Blok's prototype, the heat exchangers have the geometric configuration of a woven screen, which is ideal for simulations. It should be noted that, it is hard to manufacture such type of heat exchangers, and therefore conventional designs such as shell-and-tube heat exchanger will be used for practical designs. In this paper, we mainly focus on the numerical analysis, and therefore it is more convenient to use the same type of heat exchangers as those in de Blok's prototype. In table III, AHX1, REG1 and HHX1 form the thermoacoustic core for the engine, while AHX2, REG2 and CHX2 form the thermoacoustic core for the cooler. In de Blok's prototype, the gap between the two engine stages is about 3 cm to act as a thermal buffer tube as his hot heat exchanger has a temperature less than 160 ˚C. In our system, the temperature difference between HHX1 and AHX2 is more than 200 ˚C, and therefore, a long thermal buffer tube with a length of 12 cm is required to reduce the heat losses.

The optimisation processes are very tedious and are omitted in this paper. The results based on the final model after the optimisation have been presented here, while some optimisation steps will also be presented and discussed later in this section.

Table III.Dimensions of integral system.

Part	Diameter (m)	Length (m)	R_h (um)	Porosity
REG1	0.138	0.02	40	0.77
REG2	0.138	0.02	40	0.77
AHX1	0.138	0.001	200	0.8
AHX2	0.138	0.001	200	0.8
HHX1	0.138	0.001	400	0.8
CHX2	0.138	0.001	600	0.8
	Diameter (m)		Length (m)	
Bypass	0.0586		1.32	
Resonator	0.0713		3.1478	
Inertance	0.0422		1.35	
Compliance	0.1009		0.124	
Duct between two stages	0.0504		0.12	

The final simulation results are summarised and listed in Table IV. The heat source temperature (i.e. the solid temperature at HHX1) is 260 ˚C, and heat sink temperature (i.e., the solid temperature of AHX1 and AHX2) is 28 ˚C. The net acoustic power production from the engine unit is the difference of the inlet and lout let acoustic power, and is about 394 W. The net acoustic power consumed by the cooler is 300 W. The heat input to the engine's hot heat exchanger is 1480 W. The engine efficiency η_e is defined as the ratio of the acoustic power consumed by the cooler over the heat input to the engine, and there is 20.2%, which is about 46.5% of the Carnot efficiency at this temperature range. The cooler removes 639 W heat at -19 ˚C, and rejects it at 28 ˚C. the cooler's coefficient of performance (COP) is defined as the ratio of the heat absorbed at CHX2 over the acoustic power it consumes, and therefore is about 2.13, which is 39.6% of the Carnot COP at this temperature range.

Table IV.Summary of simulation results

Symbol	Definition	Unit	Engine	Cooler
T_h	Solid Temperature at HHX1	˚C	260	--
T_a	Solid Temperature at AHX1&2	˚C	28	28
T_c	Solid Temperature at CHX2	˚C	--	-19
$W_{a,\,in}$	Acoustic power inlet	W	700	1091
$W_{a,\,out}$	Acoustic power outlet	W	1093	792.3
$W_{a,\,net}$	Net acoustic power production (engine) or consumption (cooler)	W	394	300
$Q_{in,i}$	Heat input to HHX (engine) or CHX (cooler)	W	1480	639
η_e	Engine Efficiency	%	20.2	
COP	Coefficient of performance		2.13	
η_{Carnot}	Carnot Efficiency	%	43.5	
$COPC$	Carnot COP		5.4	
η_r	Ratio to Carnot Efficiency	%	46.5	
$COPR$	Ratio to Carnot COP	%	39.6	

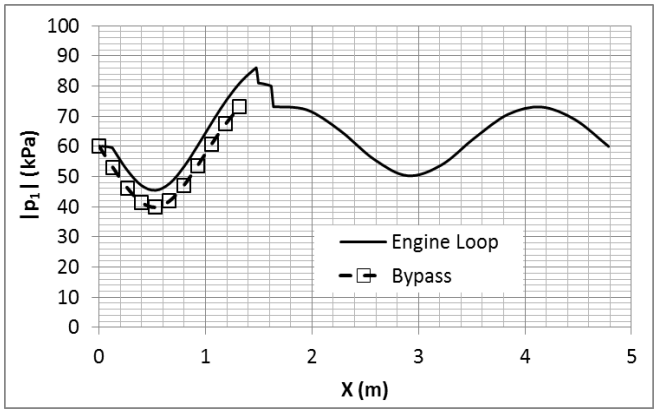

Fig. 6. Distribution of the amplitude of acoustic pressure along the loop.

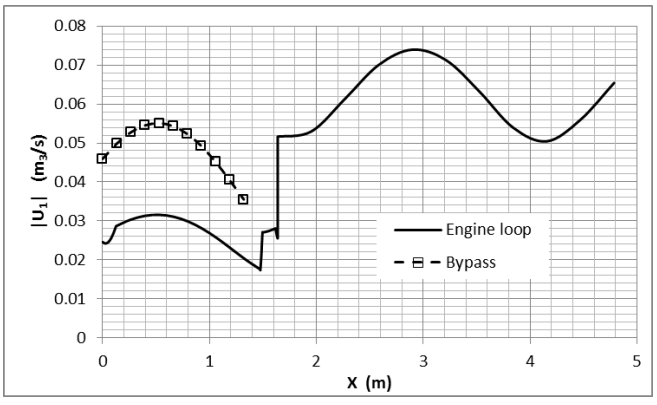

Fig. 7. Distribution of the amplitude of volumetric velocity along the loop.

To further investigate the implementation of the design strategy of this type of thermoacoustic engine, the details of

ISBN: 978-988-19253-5-0
ISSN: 2078-0958 (Print); ISSN: 2078-0966 (Online)

the acoustic field within the whole system have been extracted from the simulation results and shown in Figs 6-9. In these figures, the solid line represents the results for engine loop (engine branch and feedback pipe), and the dashed line with symbols represent the results for bypass.

Figure 6 presents the acoustic pressure distribution along the system. The maximum value of pressure is 88 kPa at the engine core and the minimum value is 40 kPa at the middle of the bypass pipe, so the Standing Wave Ratio (SWR) is about 2.2 in the whole system, which is relative high compared with de Blok's prototype. This is mainly due the regenerator length having been increased to 20 mm, and therefore the flow resistance at the engine core is very high and thus the acoustic reflection is high as well. However, the situation in the feedback pipe is much better. The maximum pressure amplitude is about 72 kPa, and the minimum amplitude is about 50 kPa, so the SWR is about 1.2 which is very close to the ideal travelling wave condition (SWR=1).

Figure 7 shows the distribution of the amplitude of volumetric velocity along the system. It can be seen that the bypass pipe shunts away two thirds of the volumetric velocity at the end of the feedback pipe (X=0). This also reflects the fact that almost two thirds of the acoustic power (i.e., 1100 W) shunts to the bypass and only 727 W acoustic flows back into the engine branch. There is a sharp increase of volumetric velocity at the regenerator of engine stage due to the steep temperature gradient along the regenerator. The other sharp increase is due to the bypass pipe joining after the end of cooler.

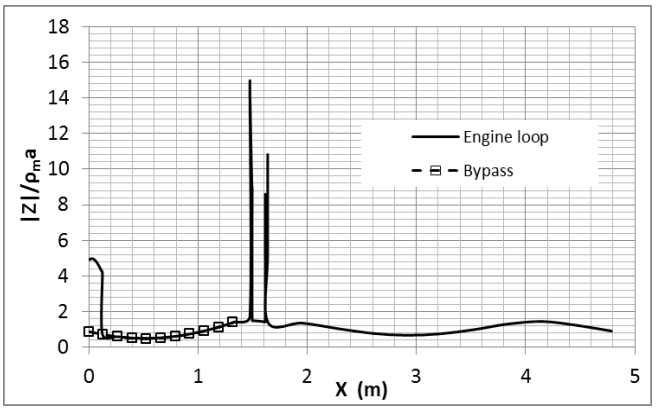

Fig. 8. Distribution of the normalized acoustic impedance along the loop.

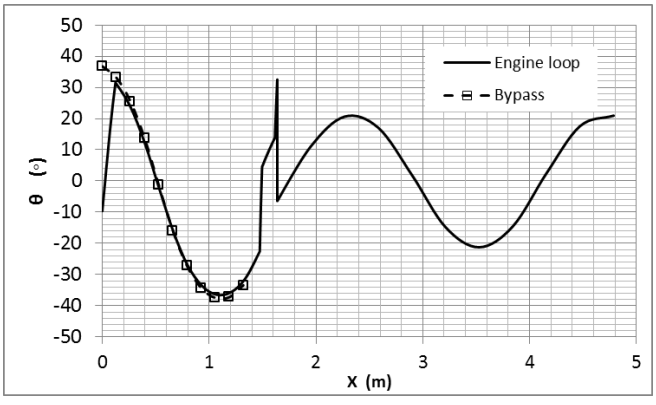

Fig. 9. Phase angle θ between pressure and velocity oscillations along the loop.

Figure 8 shows the normalised acoustic impedance along the system. As well known, to reduce the acoustic losses with in the regenerator, the impedance should be designed in the range of 15-30 times of $\rho_m a$ [5]. In the present design, it can be seen that the normalised acoustic impedance in most parts of the system is around 1 except the engine stage and cooler sections where it is 15 and 12 respectively. It should be noted that de Blok's original design deliberately have a low impedance within the regenerators by reducing the length of the regenerator to achieve a very low onset temperature difference. In our design, we focus on the efficiency and also want to use a heat source with a relative higher temperature. Therefore, a relatively long regenerator is required. In this way, the design principle of Backhaus' prototype is utilised here. It is very interesting that both of these two principles can be achieved in one system.

Figure 9 shows the phase difference between pressure and velocity oscillation along the loop. It can be found that phase angle is in the range $-20° < \Theta < 20°$ in the feedback pipe, and engine and cooler sections, which are exactly the design target. The rest of the system also has a phase angle in the range $-40° < \Theta < 40°$.

IV. Further Analysis and Discussion

The optimization needs to sweep a large group of parameters. To further understand the design of this complicated system as shown in the section III, a few typical optimization steps are presented here. The inertance tube, bypass pipe and the regenerators of engine and cooler are the most important design parameters, and therefore are selected to demonstrate the optimization processes.

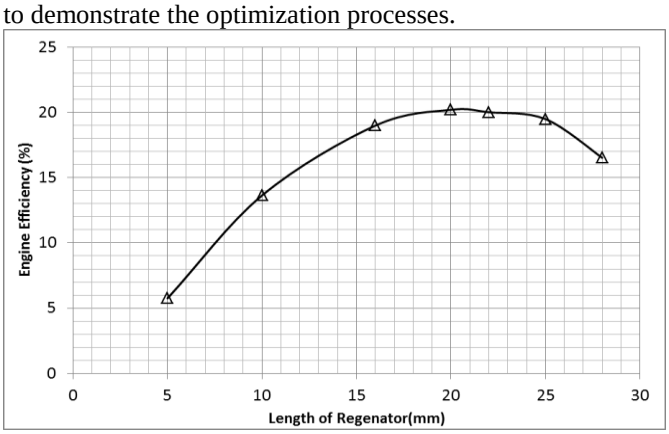

Fig. 10. Engine efficiency vs. length of engine's regenerator.

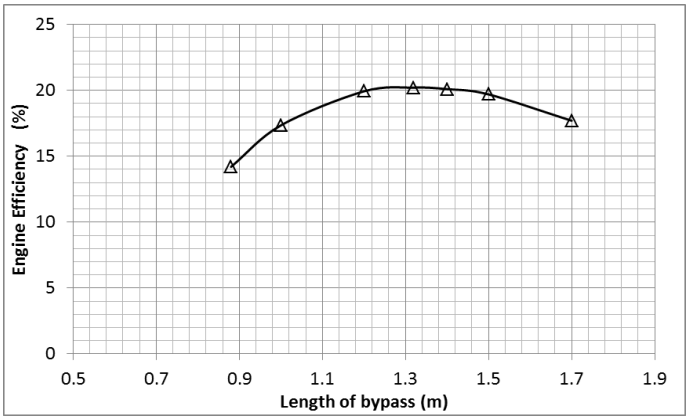

Fig. 11. Engine efficiency vs. length of bypass pipe.

ISBN: 978-988-19253-5-0
ISSN: 2078-0958 (Print); ISSN: 2078-0966 (Online)

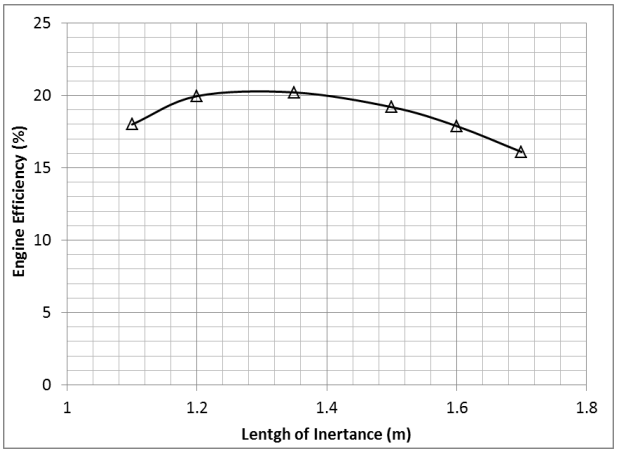

Fig. 12. Engine efficiency vs. length of inertance tube.

Figure 10 shows effect of the length of the regenerator in the engine unit on the engine efficiency. It can be found that there is an optimal regenerator length of about 20 mm, which is selected the final design as sumarrised in Table 3. The regenerator length is very crucial. The flow reistance increases when the length increases. For a given temperature difference, the longer the length, the smaller thetemprature gradient and consequently the less power production. On the other hand, the shorter the length, the higher the conductive heat loss through the regenerator, and therefore a tradeoff is required.

Figure 11 shows the relationship between the engine efficiency and length of the bypass length. The optimal length is about 1.3 m and is chosen for final design. Similarly, Fig. 12 shows the relationship between the length of the inertance tube and engine efficiency. The optimal length is about 1.3 m, and is selected for our final design. The bypass and inertance tube are both the phase tuning components. Their dimensions are very sensitive to achieve the right phase and impedance within the engine and cooler units and the feedback pipe.

According to the results shown in Section III and IV, it can be found that the design strategies proposed by de Blok and Backhaus can be both implemented in our travelling wave thermoacoustic engine driven cooler system.

V. CONCLUSION AND FUTURE WORK

This paper presents a comprehensive numerical analysis of hybrid configuration travelling wave thermoacoustic engine driven cooler. The numerical model was first established based on the reported prototype, and validated by the published experimental data. The design principle is then fully understood based on the analysis of the acoustic field within the engine. The validated model is then applied to design a thermally driven travelling wave thermoacoustic cooler with hybrid configuration. The design principles contained in the hybrid configuration have been implemented in our design successfully although the design objectives have been changed to achieve higher efficiency and a cooler stage is introduced to the engine to act as acoustic load. It is found that the design strategy for a high efficiency engine can be incorporated in our design. The research results showed that the new system can achieve about 46.5% of the Carnot efficiency and 39.6% of the Carnot COP. It can be expected that a better performance can be achieved if the pressurised helium is used as the working medium.

The prototype based on this design is currently under construction. The experimental results will be obtained and reported in the near future.

REFERENCES

[1] Ceperley PH: A pistonless Stirling engine-The traveling wave heat engine. *The Journal of the Acoustical Society of America* 1979, 66:1508.

[2] Ceperley PH: Gain and efficiency of a short traveling wave heat engine. *The Journal of the Acoustical Society of America* 1985, 77:1239.

[3] De Blok K: Novel 4-stage traveling wave thermoacoustic power generator. In: *Proceedings of ASME: 2010*; 2010: 1-8.

[4] Yazaki T, Iwata A, Maekawa T, Tominaga A: Traveling wave thermoacoustic engine in a looped tube. *Physical Review Letters* 1998, 81(15):3128.

[5] Backhaus, S. and Swift, G.W., A thermoacoustic- Stirling heat engine: Detailed study, Journal of Acoustical Society of America, vol 107(6), pp 3148-3166, 2000.

[6] Tijani, M. E. H. and Spoelstra, S. A high perfprmance thermoacoustic engine. J. Appl. Phys. 110:093519, 2011.

[7] De Blok K, Systemen AT: Multi-stage traveling wave thermoacoustics in practice. In: 19th International Congress on Sound and Vibration Vilnius, Lithuania: International Institute of Acoustics and Vibration (IIAV) and Vilnius University: *2012*; 2012: 1-8.

[8] De Blok, K., Low operating temperature integral thermo acoustic devices for solar cooling and waste heat recovery. Journal of the Acoustical Society of America, 2008.123(5): p. 3541-3541.

[9] Ward B, Clark J, Swift G: Design environment for low-amplitude thermoacoustic energy conversion, DELTAEC version 6.2: Users guide. *Los Alamos national laboratory* 2008.

[10] De Blok CM. Thermoacoustic system Dutch patent. International application number PCT/NL98/00515; 1998.

ISBN: 978-988-19253-5-0
ISSN: 2078-0958 (Print); ISSN: 2078-0966 (Online)